Intracellular Nanoparticle Coating Stability Determines Nanoparticle Diagnostics Efficacy and Cell Functionality

*Stefaan J. H. Soenen, Uwe Himmelreich, Nele Nuytten, Thomas R. Pisanic II, Aldo Ferrari, and Marcel De Cuyper**

Iron oxide nanoparticles (NPs) are frequently employed in biomedical research as magnetic resonance (MR) contrast agents where high intracellular levels are required to clearly depict signal alterations. To date, the toxicity and applicability of these particles have not been completely unraveled. Here, we show that endosomal localization of different iron oxide particles results in their degradation and in reduced MR contrast, the rate of which is governed mainly by the stability of the coating. The release of ferric iron generates reactive species, which greatly affect cell functionality. Lipid-coated NPs display the highest stability and furthermore exhibit intracellular clustering, which significantly enhances their MR properties and intracellular persistence. These findings are of considerable importance because, depending on the nature of the coating, particles can be rapidly degraded, thus completely annihilating their MR contrast to levels not detectable when compared to controls and greatly impeding cell functionality, thereby hindering their application in functional in vivo studies.

1. Introduction

In the past two decades, improvements in physical and material sciences have revolutionized the area of nanotechnology, providing fascinating new tools such as scanning probe microscopy, which allow scientists to accurately investigate a broad spectrum of physical properties that were previously hard to analyze.[1] The increase in knowledge of nanophysics and materials science has led to further discoveries in biology and medicine,[2] initiating the rise of an exciting scientific discipline: nanomedicine.[3] One key aspect of nanomedicine is the development of novel or the improvement of already existing (multimodal) nanoparticles (NPs; solid colloidal particles), which can be used for biomedical imaging, drug or gene delivery, and cancer therapy.[4] Some commonly used NPs in biomedical research are quantum dots; carbon nanotubes; and gold, silver, and iron oxide NPs.[5]

Dr. S. J. H. Soenen,[+] N. Nuytten, Prof. M. De Cuyper
Subfaculty of Medicine
Katholieke Universiteit Leuven – IRC
KUL–Campus Kortrijk, Lab BioNanoColloids
E. Sabbelaan 53, 8500 Kortrijk, Belgium
E-mail: Marcel.Decuyper@kuleuven-kortrijk.be

Prof. U. Himmelreich
Faculty of Biomedical Sciences
Katholieke Universiteit Leuven Campus Gasthuisberg
University Medical Hospital Gasthuisberg
MoSAIC/Biomedical NMR Unit
Herestraat 49, 3000 Leuven, Belgium

Dr. T. R. Pisanic II
MagneSensors, Inc.
Pacific Heights Blvd 9717-A, 92121 San Diego, CA, USA

Dr. A. Ferrari[+]
Scuola Normale Superiore di Pisa
NEST-lab (National Enterprise for nanoScience and nanoTechnology)
Piazza San Silvestro 12, I-56127 Pisa, Italy

[+] Current address: Faculty of Pharmaceutical Sciences, University of Gent, Laboratory of General Biochemistry and Physical Pharmacy, Harelbekestraat 72, 9000 Gent, Belgium

[++] Current address: ETHZ, Lab of Thermodynamics in Emerging Technologies, Sonneggstrasse 3, CH-8092, Zurich, Switzerland

DOI: 10.1002/smll.201000763

NANO MICRO small

One of the most promising biomedical applications of NPs is the in vitro labeling of stem or immune cells, enabling the ability to noninvasively track their migration upon transplantation in vivo.[6] For biomedical applications, these particles require a stable coating, which renders them soluble in physiological buffer and shields the often toxic components of the particle core (e.g., heavy metals) from the cellular microenvironment.[7] The potential toxicity of nanomaterials has substantially increased the number of studies addressing NP-mediated toxic effects.[8] The wide variety in composition and size of the NPs used, their specific surface chemistry, the variety in cell types tested, and variations in protocols for cell exposure, govern both toxic effects and internalization efficiencies and and have made it near impossible to draw any general conclusions regarding the safety of the NPs used.[9]

To reduce NP-mediated cytotoxicity, various coatings, including natural (dextran) or synthetic (polystyrene) polymers, amphiphiles (lipids), or small molecules (citrate) are applied, since reduced interactions with the cell surface can diminish toxic effects, but such coatings also impede NP internalization.[7] To date, novel iron oxide formulations are often thoroughly characterized with regard to their physicochemical properties, and more recently, the interactions of these NPs with biological systems are also gaining more attention.[10] One aspect that has not received adequate attention is the intracellular fate of the particle and several questions remain, for example: 1) whether internalized particles will remain intact even after long periods of time, 2) how this might affect cell functionality and NP characteristics, and 3) whether these particles are, in fact, suitable for biomedical research and safe enough to be used in clinical trials using in vitro labeled cells.

2. Results and Discussion

2.1. Effect of pH-Dependent NP Degradation on MR Contrast

In the present work, four different types of iron oxide NPs are chosen as model systems: FDA-approved Endorem (called Feridex in the US; dextran-coated), Resovist (carboxydextran-coated), very small organic particles (VSOP; citrate-coated[11]), and cationic magnetoliposomes (MLs; lipid-coated[12]) (see Supporting Information, Table S1 for an overview of their most important physicochemical characteristics). Endorem is the most commonly used iron oxide formulation for in vitro cell labeling and recently, clinical trials regarding the magnetic resonance imaging (MRI) monitoring of Endorem-labeled cells in vivo have been set up.[13] Resovist has been extensively studied as an optimized formulation with increased uptake efficiencies, and VSOPs are undergoing clinical trails. MLs, i.e., iron oxide cores each individually wrapped in a (phospho)lipid bilayer, have recently been put forward as highly efficient in vivo imaging and therapeutic agents[14] and cationic MLs were put forward by our group as universal agents for efficient in vitro cell labeling.[15] Upon exposure to biological cells, all of these particles have been described to enter the cell by endocytosis, ultimately arriving in the endosomal compartments of the cell.[16] During endocytosis, the NPs are exposed a pH decreasing from 7.4 in the extracellular environment to 6.0 in the early endosomes, then to 5.5 in the late endosomes, and finally to 4.5 in the lysosomes.[17]

To assess the effect of the pH conditions of the lysosomal microenvironment on NP stability, the particles were exposed to citrate-containing buffers with pH 7.0, 5.5, and 4.5, as described by Arbab et al.[16b] **Figure 1**a–c shows a pH-dependent release of ferric ions, which is maximal at pH 4.5. The number of ferric ions released varied greatly between the different particles. The maximum number was released by citrate-coated VSOPs, which started to degrade at pH 7.0 and were completely degraded after one week at pH 4.5. The other particles were more resistant, with MLs degrading the least. These findings are also reflected in the T_2* relaxation times measured on samples exposed to identical conditions (Figure 1h–k). For MLs and Endorem, a slight increase in the T_2* relaxation time was observed after 2 weeks of exposure to pH 4.5, whereas the degradation of the VSOPs increased their T_2* relaxation time to levels that were not discernibly different from particle-free controls after 1 week. The findings for dextran-coated particles agree with those reported by Arbab et al.,[16b] who also observed a pH-dependent degradation with time. The above-mentioned findings bring into question the use of rapidly degrading particles for long-term cell tracking in vivo because in addition to the dilution of particles in actively proliferating cells, which has previously been found to be a major obstacle,[18] intracellular degradation of the NPs will render them impossible to detect.

2.2. Cellular Endocytosis and Intracellular Localization of NPs

The intracellular degradation of the particles may have profound effects on cellular homeostasis because iron is involved in cellular processes, such as cell cycle progression, and the ferric ions may generate reactive species (ROS) when present in the lysosomal microenvironment.[19] To evaluate the effects of intracellular NP degradation in cells, C17.2 neural progenitor cells (NPCs), a highly proliferative v-myc transduced neural progenitor cell line, and rat pheochromocytoma cells (PC12), transformed cells which under specific stimulation reproduce most of the aspects of the neuronal differentiation process,[20] were exposed to the selected particle formulations. These cells were selected based on the great interest in and large number of studies employing neural stem or progenitor cells in iron oxide NP labeling studies to enable noninvasive monitoring of any migration of these stem cells upon implantation in the brain of neurodegenerative disease models.[18] To allow comparison between the various NPs, incubation conditions were modified until similar intracellular iron oxide levels were achieved after the same incubation period (**Figure 2**a-b; see Experimental Section for incubation protocols). For C17.2 NPCs, all particles reach intracellular levels of about 40 pg Fe per cell and are nicely internalized, as can be clearly observed through the formation of a perinuclear ring that is apparent in the optical microscopy images of diaminobenzidine-enhanced Prussian

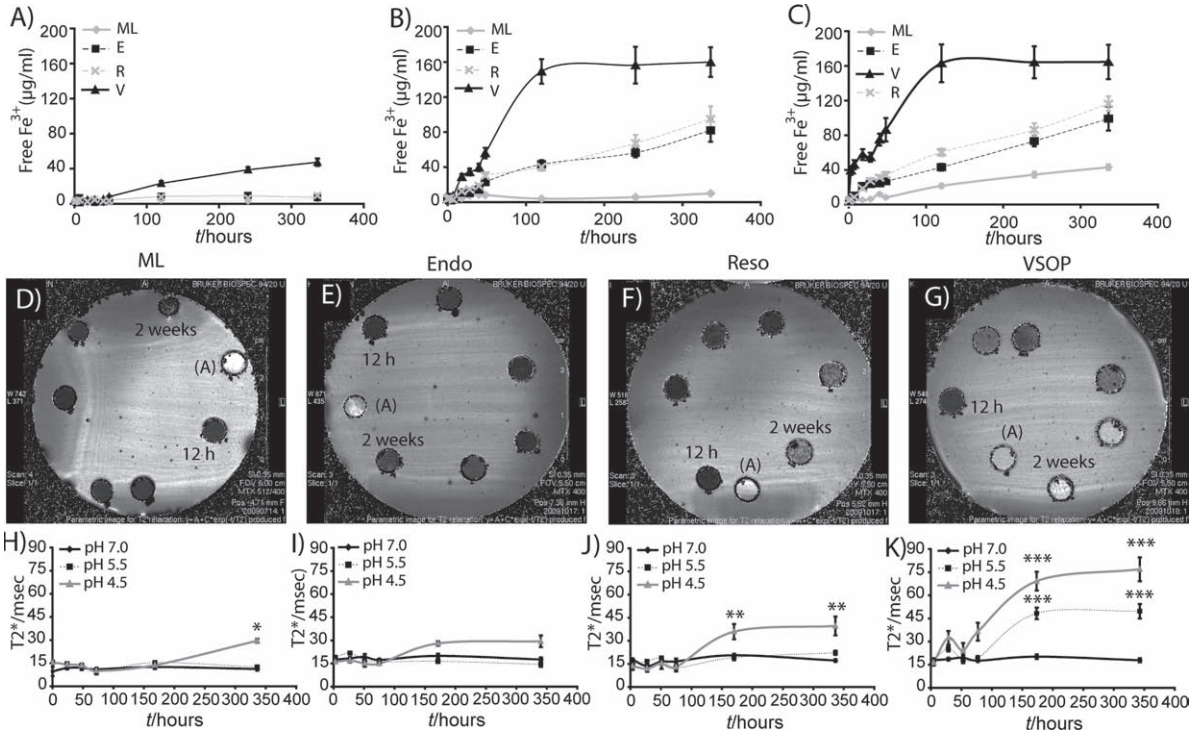

Figure 1. pH effect on particle degradation and MR signal intensities. The amount of free ferric iron measured as a function of time for the 4 NPs (MLs, Endorem, VSOP and Resovist) incubated at 200 µg Fe mL^{-1} in 20 mM sodium citrate containing cell culture medium at different pH values: a) pH 7.0, b) pH 5.5, and c) pH 4.5; $n = 4$. Representative T_2* maps measured for NPs in the above-described medium at pH 4.5: d) ML, e) Endorem, f) VSOP, and g) Resovist. The samples were collected at different time points after addition of the NPs to the acidic culture medium and are represented clockwise in terms of increasing incubation time, starting with the labeled position (A) for pure agar, the times were 12 h, 24 h, 48 h, 72 h, 1 week, and 2 weeks. T_2* values obtained when calculating the T_2* maps of the 4 NPs are shown for h) ML, i) Endorem, j) VSOP, and k) Resovist, at pH 7.0, 5.5, and 4.5 as a function of incubation time. Significant increases in T_2* relaxation times of NPs treated at pH 5.5 and pH 4.5 compared with the values obtained at pH 7.0 are seen (*: $p < 0.05$; **: $p < 0.01$; ***: $p < 0.001$).

blue stained cells (Figure 2c–g). For PC12 cells, the amount of iron is significantly lower due to the much smaller size of the cells and the variation in cellular particle content is larger, but not significant (Figure 2b). The amount of cytoplasm is limited and, therefore, the particles do not appear in a perinuclear ring, but are instead located close to and sometimes on top of the nucleus (Figure 2h–l). Under the conditions used, only the VSOP particles exhibited slightly toxic effects, as shown in Figure 2m–s.

As stated above, after endocytosis, all NPs reside in lysosomal compartments.[16] To ensure that under the conditions used in this study all particles follow the same endocytic pathway, the localization of the NPs (green) and Alexa Fluor 633-transferrin (red) was analyzed and demonstrated a clear colocalization (yellow) for all particles with transferrin (**Figure 3**). On the other hand, none of the particles were encorporated by endocytosis at 4 °C, indicating an active endocytosis pathway (Supporting Information, Figure S1). Taken together, this demonstrates that despite intrinsic differences in physicochemical properties and incubation conditions (e.g., the ratio of NP and transfection agent, see Experimental Section), the NPs were all routed along a clathrin-mediated endocytosis pathway. This furthermore indicates that any differences observed in cellular behavior were not caused by different localization of the NPs and that all NPs were exposed to similar intracellular microenvironments at the same time because the rate of their intracellular routing was similar.

2.3. Effects of Intracellular Nanoparticle Degradation on Cell Functionality

Upon internalization, NP-treated cells transiently generate ROS, the extent and rate of which is dependent on the type of particle used (**Figure 4**a-b). These reactive species were found to mainly be caused by the degradation of the iron oxide cores, as ROS levels decreased to near control levels upon addition of either 0.5 mM desferrioxamine, an iron chelator, or in the presence of 2 mM N-*t*-butyl-α-phenylnitrone, a free radical scavenger (data not shown). In line with the rapid pH-dependent degradation described above, VSOP particles induced maximal ROS levels after only 4 h, whereas the other particles showed a delayed and diminished effect, which is further supported by earlier literature data indicating similar NP-mediated effects on ROS generation.[11,15a,21] The ferric ions released can be shuttled out of the endosomes into the cytoplasm after binding to low molecular weight molecules, such as citrate.[16b] This will affect the labile iron pool of the cytoplasm, which normally

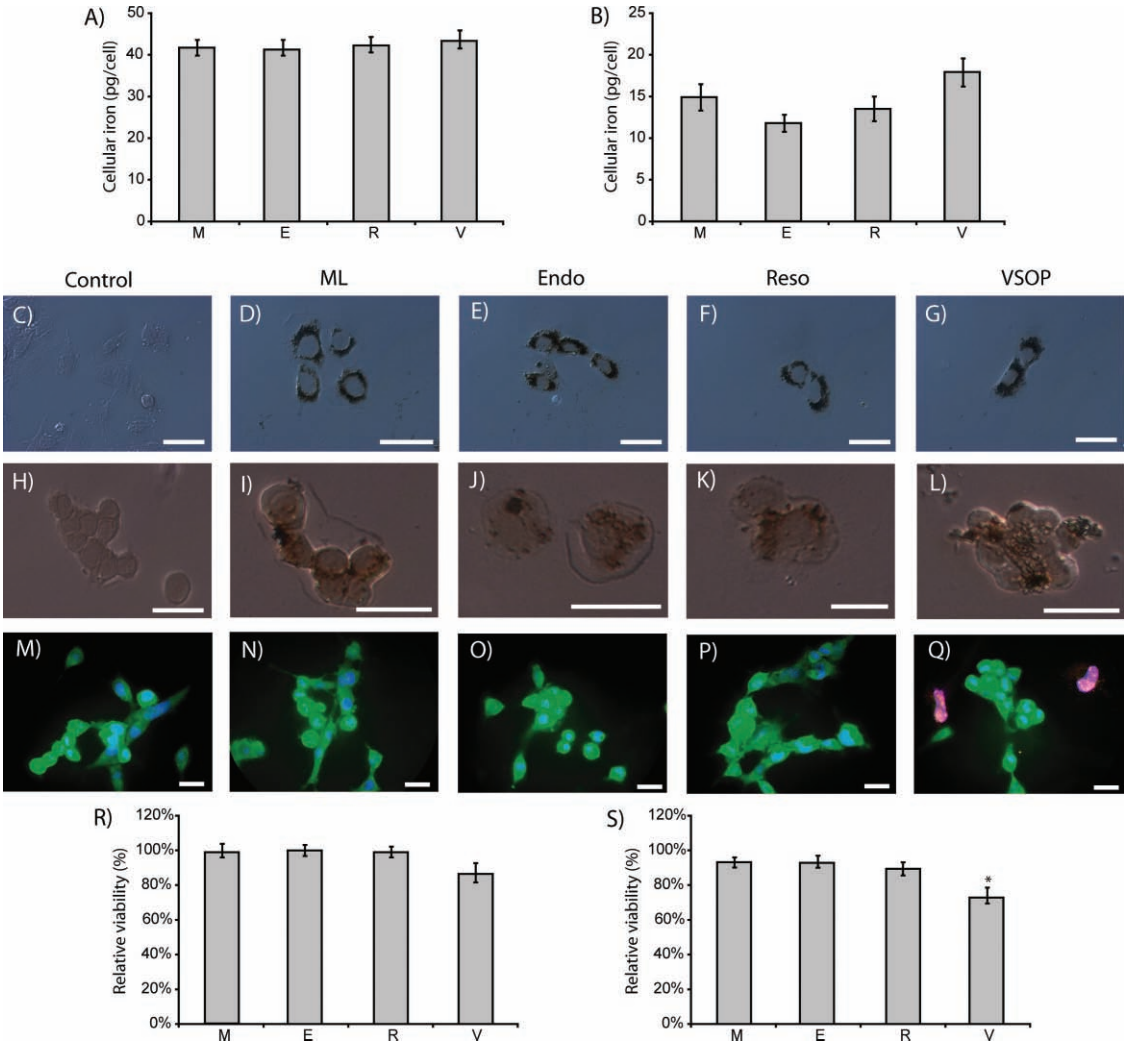

Figure 2. Nanoparticle uptake and cytotoxic effects of the 4 NPs on C17.2 neural progenitor cells and PC12 cells. Cellular iron levels of a) C17.2 and b) PC12 cells showing similar levels of intracellular iron oxide for all NPs under the conditions used. No significant differences between the different NPs were found. Representative optical microscopy images of c–g) C17.2 cells and h–l) PC12 cells stained for iron oxide using DAB-enhanced Prussian blue. A nice perinuclear staining can be noted for all NPs in both cell types (most pronounced in C17.2 cells). The images depict c,h) untreated control cells, d,i) cells treated with MLs, e,j) Endorem, f,k) Resovist, or g,l) VSOP. Scale bars: 50 µm (j) and 25 µm (k). Fluorescence microscopy images of m) untreated C17.2 cells, or cells treated with n) MLs, o) Endorem, p) Resovist, or q) VSOP, indicating cell viability by calcein AM (green, live cells) and ethidium homodimer (red, dead cells) costaining. Nuclei are counterstained using 4',6-diamidino-2-phenylindole (DAPI; blue). Scale bars: 50 µm. Relative viability of r) C17.2 or s) PC12 cells treated with the NPs at conditions yielding the intracellular iron levels shown in (a-b), as obtained from a lactate dehydrogenase assay. When appropriate, the level of significance compared with untreated control cells (100% viability) is indicated (*: $p < 0.05$).

constitutes approximately 5% of the total cellular iron content, and disrupt iron homeostasis. This was tested by measuring the expression level of transferrin receptor 1 (TfR1; Figure 4c–g), which mediates cellular iron uptake by binding transferrin, the iron transport molecule in blood.[22] Compared to control cells, all cells had increased TfR1 levels, but in agreement with the pH-dependent degradation and the ROS generation, the level of upregulation of TfR1 expression was correlated with the degradation rate of the NPs, at a maximum for VSOP particles and a minimum for MLs.

The increase in TfR1 expression is somewhat at odds with what was expected. Upon NP degradation and shuttling of iron through the divalent metal transport channel out of late endosomes and lysosomes into the cytoplasm, the cytoplasmic iron levels (the labile iron pool) increase. In response, the demand for fresh iron input from extracellular sources diminishes, which should result in lower TfR1 levels. In biological terms, the expression of TfR1 is mediated by the iron regulatory protein 1,[23] which stabilizes the messenger RNA (mRNA) of TfR1, but upon iron binding, this protein no longer binds the mRNA and the mRNA is then degraded more rapidly. Here, it is observed that rapid NP degradation and iron release increased TfR1 levels, as was also previously reported.[22] Other groups have, however, observed a decrease in TfR1 expression.[24] Studying cellular iron homeostasis is very delicate because TfR1 levels are influenced by the rate of cell turnover.[25] Therefore, after labeling, C17.2 cells were kept in culture under identical conditions, where cell densities

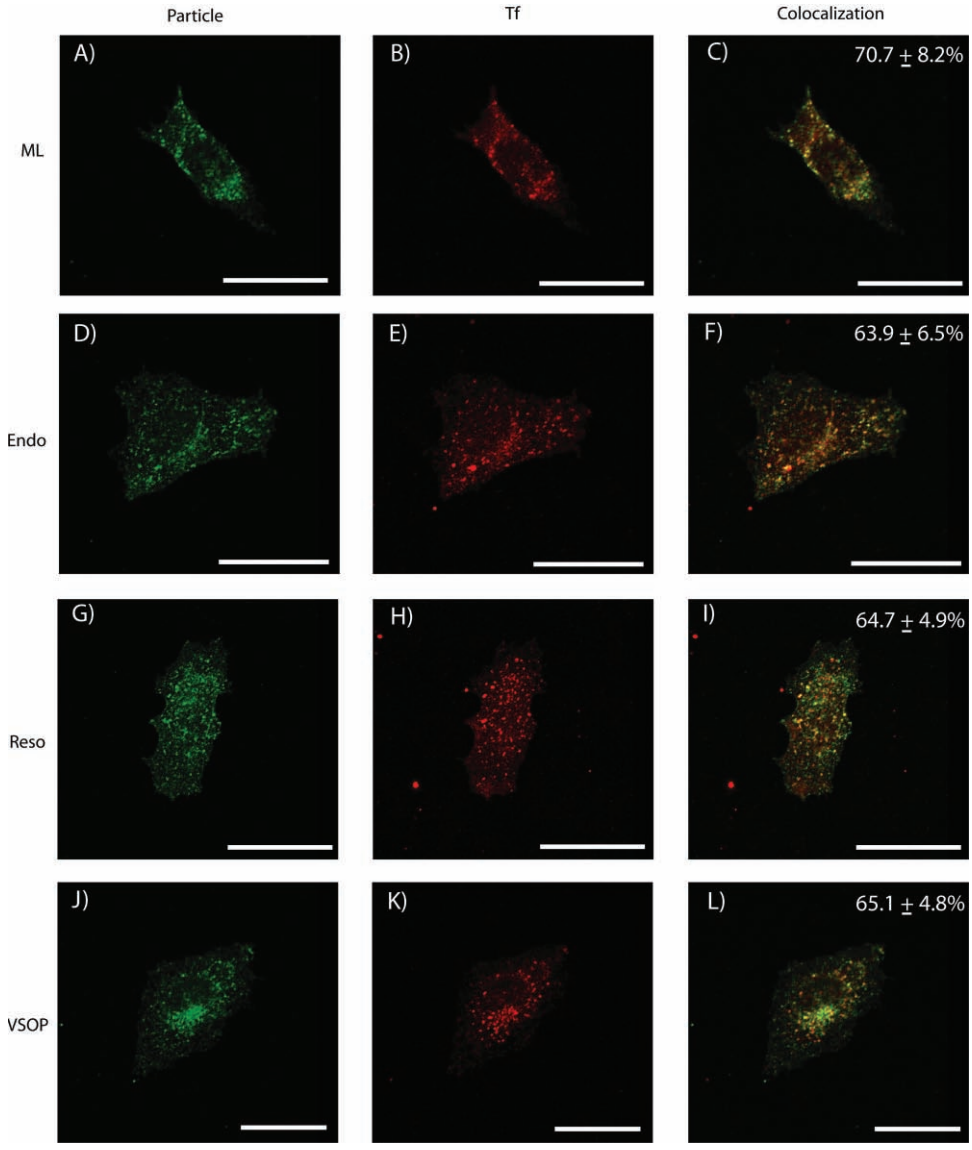

Figure 3. Intracellular nanoparticle routing. Representative confocal images of C17.2 cells incubated with a) MLs, d) Endorem, g) Resovist or j) VSOP and Alexa Fluor 633 conjugated transferrin (red; b,e,h,k) for 1 h at 4 °C (allows binding, but inhibits active endocytosis) followed by 10 min incubation at 37 °C (enables active endocytic uptake of bound NPs and transferrin). Panels (c), (f), (i), and (j) are merged images of the respective green and red channels, showing high degrees of colocalization (yellow) for all particles under the conditions used. The values indicated in the top right corner indicate the percentage of colocalization ± standard deviation.[36] Scale bars = 50 μm.

and cell cycle progression were carefully monitored and found to be equal in all samples (data not shown). It is possible that the TfR1 expression increase or decrease may be cell type dependent,[24] but it might also be time dependent. Initially, the labile iron pool may increase, lowering the TfR1 expression and increasing expression of ferritin, the iron storage protein. With time, the rate of NP degradation and the amount of iron transferred to the cytoplasm would then decrease. In turn, this may affect iron transport and because ferritin levels would still be elevated, the demand for iron input would be higher than normal, resulting in above normal TfR1 expression levels.

Common stem cell differentiation protocols suffer several drawbacks which make them less suited for assessing the effect on cell functionality. Pisanic et al.[7] developed a quantifiable model cell system where, after NP labeling, the capacity of PC12 cells to respond to their putative biological cue, i.e., nerve growth factor (NGF), can be analyzed. After 2 days of NGF treatment, neurite extension was analyzed (**Figure 5**a–e) and indicated severely impaired functionality of VSOP-labeled cells. The total number (Figure 5k) and the average length of the neurites per cell (Figure 5l) were significantly reduced when the cells were incubated with NPs; cells were most affected by VSOP particles. After 6 days of NGF-treatment, the neurites had branched out, establishing intercellular contacts (Figure 5f–j,m). In accordance with the data obtained above, a clear correlation between the impairment of neurite branching and the intracellular stability of the particles can be noted, with branching being least affected by MLs and most affected by VSOP. Neurite branching is vital

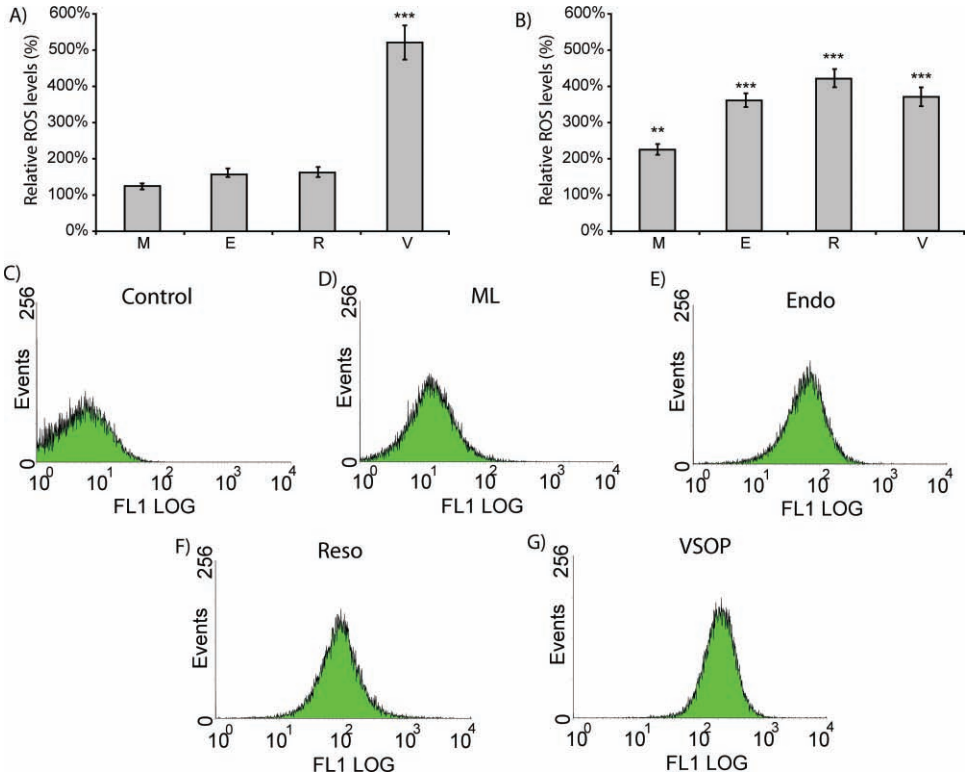

Figure 4. Effects of intracellular NP degradation on cell physiology. Relative levels of ROS in C17.2 cells at a) 4 h and b) 24 h incubation with the respective NPs. When appropriate, the degree of significance when compared with ROS levels in untreated control cells (100%) is indicated (*: $p < 0.05$; **: $p < 0.01$; ***: $p < 0.001$). Flow cytometric analysis of TfR1 expression in c) untreated control cells or cells incubated with d) MLs, e) Endorem, f) Resovist, or g) VSOP at 1 week of continuous culture post NP-exposure, where there were no differences in proliferation rates or cell densities between the different groups. Expression levels were normalized using isotype control antibody.

for establishing neuronal connections and its disruption is known to hamper neuronal functionality both in vitro and in vivo.[7]

Very recently, several other studies have also reported on the importance of NP localization and the effects on NP degradation.[26] For instance, in the study by Lee et al.[26b] it was observed that superparamagnetic iron oxide cores encapsulated in biodegradable poly(D,L-lactic-co-glycolic acid) cores and positively charged chitosan shells ended up in liver cells after intravenous injection. After endosomal and lysosomal accumulation of the particles, it was noted that these particles were gradually broken down, which significantly impeded the T_2* contrast generated by the labeled liver cells. This agrees completely with the findings of the present study, where endosomal localization leads to a gradual degradation of all iron oxide NPs tested. The rate of degradation appears to be related to the resistance of the coating molecules to the acidic environment. The degradation of the coating is in itself harmless, but when it results in exposure of the NP core to the acidic environment, toxic effects can be induced. This agrees with the study by Lehmann et al.[26c], where it was observed that when iron-platinum NPs embedded in a poly(methacrylic acid) polymer shell were exposed to dendritic cells, macrophages, and epithelial lung cells, the proinflammatory response elicited by the particles was correlated to their precise intracellular localization. Furthermore, by comparing particles with the mere polymer shell, it was observed that the core and not the shell led to the observed effects.

2.4. Effect of ML Clustering on MR Contrast and Labeling Durability

Interestingly, the data mentioned above show that MLs appear to be the least susceptible to degradation, indicating that the coating is very stable and efficiently shields the encapsulated iron oxide core from the extracellular environment. Previously, MLs were also shown to remain present at detectable levels in proliferating cells for more than 20 passages, which by far exceeds the values reported for dextran-coated particles (5–7 passages).[18] In lysosomes, where the particles finally reside, lipidic structures such as liposomes, are broken down by the action of phospholipases, such as phospholipase A_2 (PLA_2). The activity of PLA_2 on the ML coating is shown in **Figure 6**a, where the pH is plotted as a function of time. The release of fatty acids acidifies the ML medium, causing a decrease in pH for PLA_2-treated particles (gray) compared with untreated MLs (black). Upon exposure to PLA_2 followed by magnetic fractionation, the ratio of µmol phosphate to milligrams magnetite steadily decreased with time (Figure 6b), ranging from 1.27 ± 0.22 to 0.47 ± 0.14 after 48 hours and 33.04 ± 0.13 after 120 hours. After 48 hours, the ratio decreased to 37.06% of the original value,

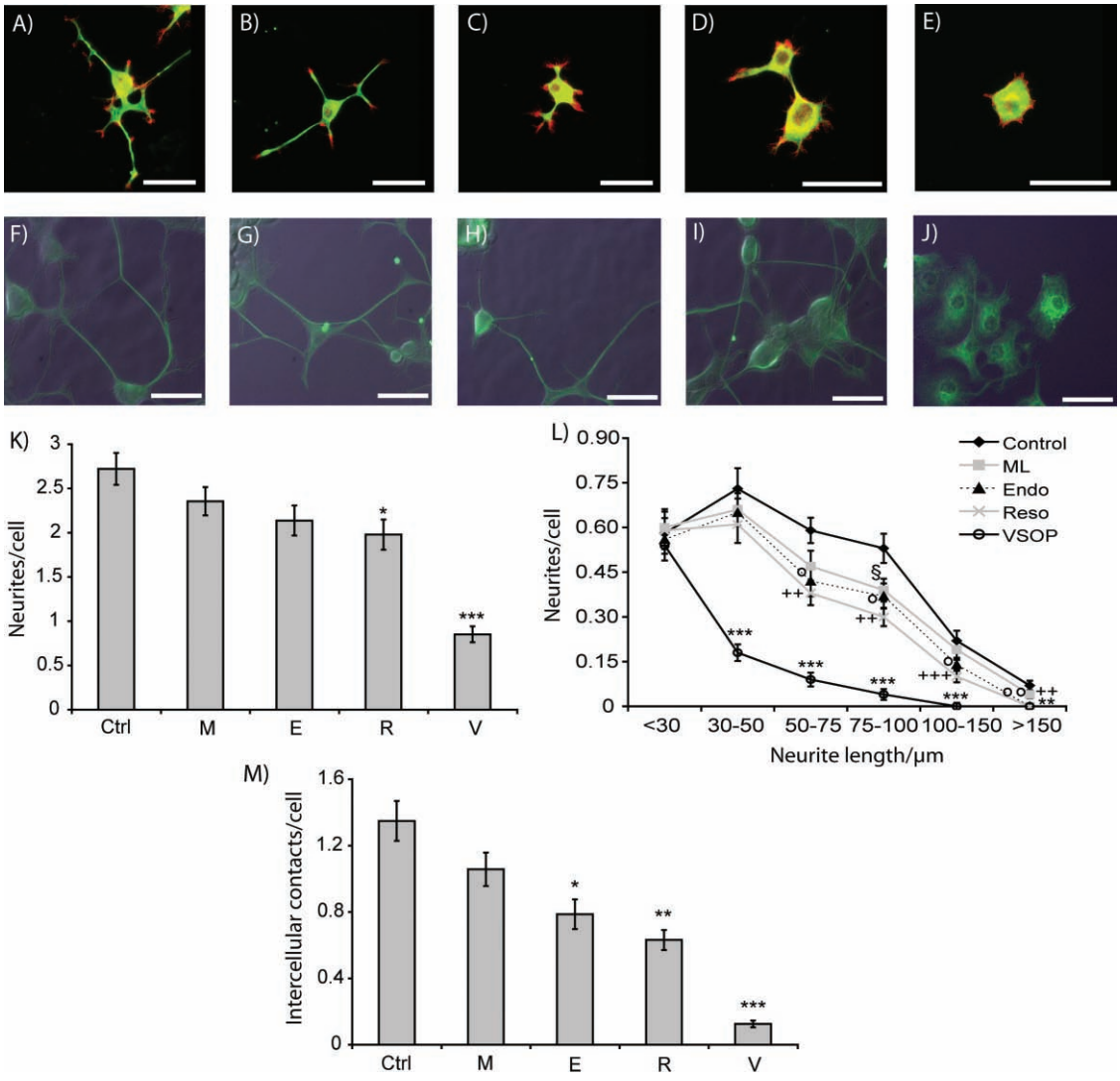

Figure 5. Effects of intracellular NP degradation on cell functionality. Representative microscopy images of PC12 cells after 2 days (a–e) or 6 days (f–j) of NGF-exposure. a–e) Fluorescence microscopy images showing α-tubulin (green) and g-actin (red) staining. f–j) Merged fluorescence, showing α-tubulin (green) and optical microscopy images. Scale bars = 50 µm. Untreated control cells are shown in (a,f), NP-treated cells are shown for cells incubated with b,g) MLs, c,h) Endorem, d,i) Resovist, or e,j) VSOP. k) The number of neurites per cell, l) the number of neurites of a certain length per cell after 2 days of NGF exposure, and m) the number of intercellular contacts per cell for control cells and NP-treated PC12 cells after 6 days of NGF exposure. When appropriate, the degree of significance when compared with untreated controls cells is indicated (*: $p < 0.05$; **: $p < 0.01$; ***: $p < 0.001$); for clarity, the degree of significance is indicated with different symbols for every type of NP in (l): ML (§), Endorem (°), Resovist (+), and VSOP (⁎).

and it further decreased to 29.18% after 120 hours. These values closely correspond to 1/3 of the total amount of lipid which resembles the theoretical amount of lipids located in the inner lipid layer.[15a] These values also agree with the experimental values retrieved when removing the outer lipid layer using organic media, which was found to produce monolayer-coated MLs stabilized in organic solvent.[27] In total, these findings support the removal of the outer lipid layer and indicate that the inner leaflet is far more resistant to PLA_2-mediated degradation. These data can be further interpreted in light of earlier findings reported by Piret et al.,[28] who showed that a distinct hydrophobic/hydrophilic interface recognition is an essential determinant in PLA_2 activity and kinetic properties. In this respect, the destruction of the outer leaflet phospholipids does not directly pose a problem because lipids residing in the inner leaflet of the lipid bilayer are strongly chemisorbed to the iron oxide surface with their fatty acyl chains oriented outwards, presenting an inaccessible surface to PLA_2. Thus, the action of PLA_2 on MLs ultimately results in monolayer lipid-coated iron oxide cores, which are extremely unstable because they have a hydrophobic exterior that eventually causes them to aggregate in an aqueous environment. The induced clustering of the monolayer-coated MLs was proven by the observed increase in hydrodynamic particle size (Figure 6c). As PLA_2-treated samples displayed substantial aggregation when exposed to an external magnetic field (Figure 6d) in comparison with the lack of any observable aggregation for non-PLA_2-treated samples, these

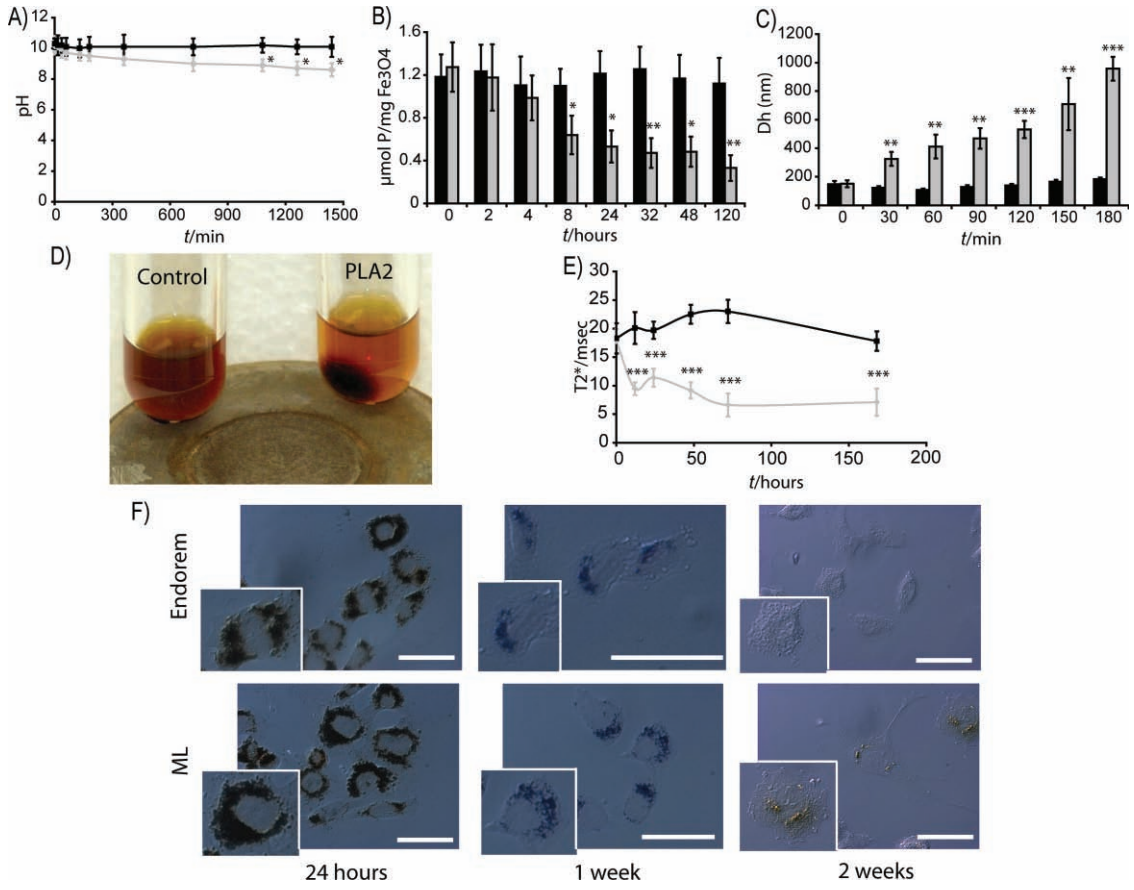

Figure 6. Clustering of magnetoliposomes. Effect of PLA_2-activity on MLs as indicated by: a) a decrease in pH of PLA_2-treated samples (gray) compared with control samples (black), b) the ratio of phosphate to magnetite for PLA_2-treated samples (gray) and control samples (black), and c) hydrodynamic diameters of PLA_2-treated samples (gray) and control samples (black). d) Optical microscopy images of control particles and PLA_2-treated particles upon exposure to a 1 T magnetic field for 30 min. e) T2* relaxation times for PLA_2-treated samples (gray) and control samples (black) indicating the enhanced effect of induced clustering of the MLs on MR contrast generation. All data are expressed as mean ± standard deviation ($n = 3$). When appropriate, the degree of significance is indicated (*: $p < 0.05$; **: $p < 0.01$; ***: $p < 0.001$). f) Representative optical microscopy images of C17.2 NPCs labeled with Endorem (top row) or MLs (bottom row) for 24 h, which finally reach similar average intracellular iron content. Media were removed and cells were kept in culture for the duration indicated. Cells were stained for iron oxide using DAB-enhanced Prussian blue and imaged 24 h (left column), 1 week (middle column), and 2 weeks (right column) post nanoparticle incubation. Scale bars: 75 µm. The insert is an enlarged view of a single cell displayed in the main image.

data further indicate that the aggregates formed possess a much stronger magnetic dipole moment.

For MR purposes, the observed clustering and the amplified magnetic dipoles result in a significant shortening of T_2* relaxation times (Figure 6e), which are most sensitive to disturbance by magnetic field inhomogeneities. The enhanced transversal relaxation caused by ML clustering would increase the contrast of the ML-labeled cells with the background and facilitate a clear depiction of the target cells. In cell-based imaging, to our knowledge, no deliberate intracellular clustering of particles has been reported to date, although extracellular clustering has been actively pursued.[29] To verify whether clustering might also occur intracellularly, C17.2 neural progenitor cells were labeled with either MLs or with Endorem, resulting in similar intracellular iron oxide levels. Cells were kept in culture, and samples were taken 24 hours, 1 week, and 2 weeks post particle incubation and stained for cellular iron (Figure 6f). At 24 hours, iron oxide levels seemed similar, whereas after 1 week, ML-treated cells appeared to contain more particles and the staining pattern was also more compartmentalized into larger 'clusters' compared with the more diffuse staining pattern of Endorem. After 2 weeks, no particles were detected for Endorem-treated cells; ML-treated cells still contained several large (µm-sized) clusters. As Endorem was the second most stable particle tested after MLs, and neither of the particles were observed to be excreted by the cells during the time span studied (data not shown), these findings further stress the extreme robustness of MLs and highlight an extremely advantageous quality of their intracellular processing. When located in the degradative endolysosomal environment, MLs cluster and the iron oxide cores are efficiently shielded from degradation, promoting their use as stable and highly efficient MR contrast agents for long-term imaging.

3. Conclusions

In this study, some of the most widely used iron oxide NPs were selected, providing a large variety in physicochemical parameters. Factors such as the core size, overall

NP size, and the available surface area are sure to influence the results. None of these parameters alone can explain the observed effects and, thus, these data indicate that the nature of the NP coating is a determining factor for the intracellular stability of the NPs. Although none of the NPs tested were completely resistant to degradation, the extent of the effects varied greatly between different particles. Depending on the envisioned application of the NPs, degradability might reduce potential long-term cytotoxic effects by clearing the NPs in vivo,[30] but it may also significantly enhance any negative effects.[31] Furthermore, for in vivo MRI of transplanted iron oxide-labeled cells, a slow degradation of iron oxide NPs might emphasize the poor correlation between MR signal and cell number upon cell death.[32] As shown here for intracellular NP delivery, NP degradation may impede both imaging and cell functionality. These data highlight the great need for more thorough cell–NP investigations where both NP efficacy and cell functionality are analyzed if these particles are to be efficiently used in biomedical research or, hopefully, transferred to clinical settings.

Of the particles tested, cationic MLs were the most resistant to degradation due to their unique features, which result in stable shielding of the iron oxide core by the strongly bound inner lipid layer. For in vivo MRI, where the amount of cellular iron is diluted exponentially upon cell divisions, high initial concentrations of iron oxide cores are beneficial for enhancing signal contrast and will allow longer in vivo visualization of the cells after transplantation.[33] High intracellular concentrations of iron oxide cores, however, have been reported to affect cell functionality and cell proliferation, have been reported to to affect the cellular cytoskeleton, and can even lead to immediate cell death.[16a,34] In this regard, larger particles (>200 nm diameter) with higher magnetic moments would lead to better MRI contrast per particle but are generally taken up very poorly by mammalian, non-phagocytic cells.[35] Thus, MLs represent ideal particles which are small enough to allow efficient uptake, but once incorporated by endocytosis, their aggregation into larger clusters results in a sustained T_2 decay.

4. Experimental Section

Nanoparticles: Resovist was purchased from Schering (Berlin, Germany), Endorem was purchased from Guerbet (Villepinte, France), VSOP (VSOP C200) was purchased from Ferropharm (Teltow, Germany), and cationic MLs (3.33% DSTAP-containing) were produced and characterized as described previously.[16a] See Supporting Information (Table S1) for an overview of the physical characteristics (size, coating, morphology, and surface properties) of the particles. For fluorescently tagged particles, FITC-labeled VSOP (VSOP C200-fluo) was obtained from Ferropharm and 0.1% 4,4-difluoro-4-bora-3a,4a-diaza-s-indacene (BODIPY FL)-containing MLs were produced as previously described.[16a]

Cell labeling: For cell internalization, the particles were diluted from stock solutions at 1000 μg Fe mL^{-1} in 0.5 mL phosphate buffered saline (PBS) (MLs), 1500 μg Fe mL^{-1} in 0.5 mL PBS (Resovist), 2500 μg Fe mL^{-1} in 0.5 mL PBS (Endorem), and 5000 μg Fe mL^{-1} in 0.5 mL PBS (VSOP). All particles, except for the already cationic MLs, were supplemented with 25 μL Lipofectamine 2000 (Invitrogen, Merelbeke, Belgium). This was done to promote cellular uptake and to induce a cationic layer which would reduce the impact of the different physicochemical properties of the NPs on cell exposure and make them more uniform, as shown in Figure 3. All mixtures (including the MLs) were incubated for 30 min at ambient temperature with light shaking to allow complex formation. Then, 4.5 mL of culture medium were added to every sample and the appropriate volume was added to the cells. The final iron concentrations for the different NPs were: 1) MLs: 100 μg Fe mL^{-1}, 2) Resovist: 150 μg Fe mL^{-1}, 3) Endorem: 250 μg Fe mL^{-1}, and 4) VSOP: 500 μg Fe mL^{-1}. For all studies, control cells were incubated with medium containing PBS (10%) to exclude any effect caused by differences in growth factors and nutrient supply.

Statistical analysis: All data are expressed as mean ± standard error of the mean (s.e.m.) unless indicated otherwise and analyzed using one-way analysis of variance (ANOVA). Multiple comparisons were analyzed using the Tukey-HSD (honestly significant difference test) post-hoc method (cellular iron content determination). When comparing the different NPs to the same control group (the reference group), the Dunnett post-hoc analysis method was used. In all cases, the degree of significance is indicated when appropriate (*: $p < 0.05$; **: $p < 0.01$; ***: $p < 0.001$).

Toxicological and MR-related experiments: Please see the Supporting Information for full methodology.

Supporting Information

Supporting Information is available from the Wiley Online Library or from the author.

Acknowledgements

S.J.S. is the recipient of a research grant from the IWT-Vlaanderen. M.D.C. and U.H. are recipients of an IWT grant-sponsoring project SBO80017. U.H. received financial support by the European Commission for EC-FP6 network DiMI (LSHB-CT-2005–512146), EC-FP7 network ENCITE (2008–201842), and the K.U. Leuven Centers of Excellence 'MoSAIC'.

[1] V. Karoutsos, *J. Nanosci. Nanotechnol.* **2009**, *9*, 6783–6798.
[2] A. Sosnik, A. M. Carcaboso, R. J. Glisoni, M. A. Moretton, D. A. Chiappetta, *Adv. Drug Delivery Rev.* **2010**, *62*, 547–559.
[3] K. Kostarelos, *Nanomedicine* **2006**, *1*, 1–3.
[4] S. Santra, C. Kaittanis, J. Grimm, J. M. Perez, *Small* **2009**, *5*, 1862–1868.
[5] a) X. Gao, Y. Cui, R. M. Levenson, L. W. Chung, S. Nie, *Nat. Biotechnol.* **2004**, *22*, 969–976; b) K. Kostarelos, L. Lacerda, G. Pastorin, W. Wu, S. Wieckowski, J. Luangsivilay, S. Godefroy, D. Pantarotto, J. P. Briand, S. Muller, M. Prato, A. Bianco, *Nat. Nanotechnol.* **2007**, *2*, 108–113; c) A. M. Gobin, E. M. Watkins, E. Quevedo, V. L. Colvin, J. L. West, *Small* **2010**, *6*, 745–752; d) J. R. McCarthy, R. Weissleder, *Adv. Drug Delivery Rev.* **2008**, *60*, 1241–1251.

[6] J. W. M. Bulte, T. Douglas, B. Witwer, S-C. Zhang, E. Strable, B. K. Lewis, H. Zywicke, B. Miller, P. van Gelderen, B. M. Moskowitz, I. D. Duncan, J. A. Frank, *Nat. Biotechnol.* **2001**, *19*, 1141–1147.
[7] T. R. Pisanic 2nd, J. D. Blackwell, V. I. Shubayev, R. R. Fiñones, S. Jin, *Biomaterials* **2007**, *28*, 2572–2581.
[8] A. Nel, T. Xia, L. Madler, N. Li, *Science* **2006**, *311*, 622–627.
[9] a) W. Jiang, B. Y. Kim, J. T. Rutka, W. C. Chan, *Nat. Nanotechnol.* **2008**, *3*, 145–150; b) V. Colvin, *Environ. Mol. Mutagen.* **2007**, *48*, 533–533.
[10] N. Lewinski, V. Colvin, R. Drezek, *Small* **2008**, *4*, 26–49.
[11] A. Stroh, C. Zimmer, C. Gutzeit, M. Jakstadt, F. Marschinke, T. Jung, H. Pilgrimm, T. Grune, *Free Radical Biol. Med.* **2004**, *36*, 976–984.
[12] S. J. Soenen, M. Hodenius, M. De Cuyper, *Nanomedicine* **2009**, *4*, 177–191.
[13] Cell tracking using superparamagnetic particles of iron oxide (SPIO) and magnetic resonance imaging (MRI) – A pilot study (US National Institutes of Health, University of Edinburgh) on www.ClinicalTrials.gov, a service of the U.S. National Institutes of Health, www.ClinicalTrials.gov. (accessed January 2010).
[14] Y. Namiki, T. Namiki, H. Yoshida, Y. Ishii, A. Tsubota, S. Koido, K. Nariai, M. Mitsunaga, S. Yanagisawa, H. Kashiwagi, Y. Mabashi, Y. Yumoto, S. Hoshina, K. Fujise, N. Tada, *Nat. Nanotechnol.* **2009**, *4*, 598–606.
[15] a) S. J. Soenen, D. Vercauteren, K. Braeckmans, W. Noppe, S. De Smedt, M. De Cuyper, *ChemBioChem* **2009**, *10*, 257–267; b) S. J. Soenen, A. R. Brisson, M. De Cuyper, *Biomaterials* **2009**, *30*, 3691–3701.
[16] a) S. J. Soenen, N. Nuytten, S. F. De Meyer, S. C. De Smedt, M. De Cuyper, *Small* **2010**, *6*, 832–842; b) A. S. Arbab, L. B. Wilson, |P. Ashari, E. K. Jordan, B. K. Lewis, J. A. Frank, *NMR Biomed.* **2005**, *18*, 383–389.
[17] B. Tycko, F. R. Maxfield, *Cell* **1982**, *28*, 643–651.
[18] P. Walczak, D. A. Kedziorek, A. A. Gilad, B. P. Barnett, J. W. Bulte, *Magn. Reson. Med.* **2007**, *58*, 261–269.
[19] D. M. Huang, J. K. Hsiao, Y. C. Chen, L. Y. Chien, M. Yao, Y. K. Chen, B. S. Ko, S. C. Hsu, L. A. Tai, H. Y. Cheng, S. W. Wang, C. S. Yang, Y. C. Chen, *Biomaterials* **2009**, *30*, 3645–3651.
[20] a) E. Y. Snyder, D. L. Deitcher, C. Walsh, S. Arnold-Aldea, E. A. Hartwieg, C. L. Cepko, *Cell* **1992**, *68*, 33–51; b) L. A. Greene, A. S. Tischler, *Proc. Natl. Acad. Sci. U. S. A.* **1976**, *73*, 2424–2428.
[21] J. W. Bulte, A. S. Arbab, T. Douglas, J. A. Frank, *Methods Enzymol.* **2004**, *386*, 275–299.
[22] R. Schäfer, R. Kehlbach, J. Wiskirchen, R. Bantleon, J. Pintaske, B. R. Brehm, A. Gerber, H. Wolburg, C. D. Claussen, H. Northoff, *Radiology* **2007**, *244*, 514–523.
[23] N. M. Sposi, L. Cianetti, E. Tritarelli, E. Pelosi, S. Militi, T. Barberi, M. Gabbianelli, E. Saulle, L. Kühn, C. Peschle, U. Testa, *Eur. J. Biochem.* **2000**, *267*, 6762–6774.
[24] E. Pawelczyk, A. S. Arbab, S. Pandit, E. Hu, J. A. Frank, *NMR Biomed.* **2006**, *19*, 581–592.
[25] R. Y. Chan, C. Seiser, H. M. Schulman, L. C. Kuln, P. Ponka, *Eur. J. Biochem.* **1994**, *220*, 683–692.
[26] a) Y.-J. Ma, H.-C. Gu, *J. Mater. Sci.: Mater. Med.* **2007**, *18*, 2145–2149; b) P.-W. Lee, S.-H. Shu, J.-J. Wang, J.-S. Tsai, K.-J. Lin, S.-P. Wey, F.-R. Chen, C.-H. Lai, T.-C. Yen, H.-W. Sun, *Biomaterials* **2010**, *31*, 1316–1324; c) A. D. Lehmann, W. J. Parak, F. Zhang, Z. Ali, C. Röcker, G. U. Nienhaus, P. Gehr, B. Rothen-Rutishauser, *Small* **2010**, *6*, 753–762.
[27] M. De Cuyper, W. Noppe, *J. Colloid Interface Sci.* **1996**, *182*, 478–482.
[28] J. Piret, A. Schanck, S. Delfosse, F. Van Bambeke, B. K. Kishore, P. M. Tulkens, M. P. Mingeot-Leclercq, *Chem. Phys. Lipids* **2005**, *133*, 1–15.
[29] T. J. Harris, G. von Maltzahn, A. M. Derfus, E. Ruoslahti, S. N. Bhatia, *Angew. Chem., Int. Ed.* **2006**, *45*, 3161–3165.
[30] M. K. Yu, Y. Y. Jeong, J. Park, S. Park, J. W. Kim, J. J. Min, K. Kim, S. Jon, *Ang. Chem., Int. Ed.* **2008**, *47*, 5362–5365.
[31] a) P. Bourrinet, H. H. Bengele, B. Bonnemain, A. Dencausse, J. M. Idee, P. M. Jacobs, J. M. Lewis, *Invest. Radiol.* **2006**, *41*, 313–324; b) T. R. Pisanic, S. Jin, V. I. Shubayev, in *Nanotoxicity: In vivo and in vitro models to health risks* (Eds: S. C. Sahu, D. A. Casciano) John Wiley & Sons Ltd, Chichester, **2009**, Ch. 20.
[32] I. Y. Chen, J. M. Greve, O. Gheysens, J. K. Willmann, M. Rodriguez-Porcel, P. Chu, A. Y. Sheikh, A. Z. Faranesh, R. Paulmurugan, P. C. Yang, J. C. Wu, S. S. Gambhir, *Mol. Imaging Biol.* **2009**, *11*, 178–187.
[33] J. R. Slotkin, K. S. Cahill, S. A. Tharin, E. M. Shapiro, *Neurotherapeutics* **2007**, *4*, 428–433.
[34] S. J. Soenen, E. Illyes, D. Vercauteren, K. Braeckmans, Z. Majer, S. C. De Smedt, M. De Cuyper, *Biomaterials* **2009**, *30*, 6803–6813.
[35] D. L. Thorek, A. Tsourkas, *Biomaterials* **2008**, *29*, 3583–3590.
[36] A. Ferrari, A. Veligodskiy, U. Berge, M. S. Lucas, R. Kroschewski, *J. Cell Sci.* **2008**, *121*, 3649–3663.

Received: May 4, 2010
Published online: September 3, 2010

